유체기계공업학회 '98 강연회 및 연구개발 발표회 논문집, pp.11-28
과학기술회관 국제회의실, 1998. 2. 18

CRACK INITIATION AND PROPAGATION OF BLADES FRACTURE MECHANICS APPROACH

J. S. Rao
Department of Mechanical Engineering
Indian Institute of Technology
New Delhi 110016

ABSTRACT

Crack initiation and propagation of blades is a serious matter in turbomachinery. Outages are common due to these problems that occur during the service of the machine resulting in a huge loss of revenue. Once in a while, the problems become serious and cause major shutdowns which can in some cases result in the loss of the whole machine in a catastrophic manner. In this presentation, we will discuss the crack initiation studies of a hydraulic machine runner blade by local stress strain approach and crack propagation at the root of a low pressure stage steam turbine blade by means of stress intensity factor approach. In both the cases, we will show how the present day technologies can predict actual field observations.

1. INTRODUCTION

A major and complete failure of starboard HP turbine blades in the ninth stage of RMS QEII occurred on 24th December 1968 during the maiden voyage of the ship from Tail O' the Bank, this was shown to be a design fault of the packetted blades by Fleeting and Coats[1]. Frank [2] reported a complete failure of B2 TG set of Electricite de France in Porschville on 22nd August 1977 while an over speed test is being conducted during the major overhaul after 25,000 hours of operation. A recent catastrophic and complete failure is one that occurred in the nuclear TG set of Narora in the early morning hours of 31st March 1993[3].

Occasionally, we have blade cracks that are initiated with the blades still intact. However, their operation becomes risky, a specific case of such an example is that of cracks that have been found at the junction of the blade and crown of a runner blade of Francis hydraulic turbines[4]

The free vibration behavior of different types of turbine blades has been amply discussed by Rao[5]. Several methods have been developed by various researchers to determine the free vibration characteristics different types of blades, e.g., 1. Energy methods[6], 2. Finite element methods based on beam elements[7], Solid elements[8] or plate or shell theories[9]. However, it becomes difficult to model complicated geometries, particularly the blade root or the shroud interfaces accurately in a short period of time. In general, recourse is then taken to commercially available FEM codes such as I-DEAS[10], which makes the modeling easier and also provide a reasonable amount of confidence in the results.

Blade excitation occurs usually at the nozzle passing frequency and is usually an aerodynamic phenomenon, see Rao[11]. Another mechanism of excitation is due to mechanical assembly errors of the diaphragms in the stator ring, the first six engine harmonics are important. Measurements[12] indicate that the magnitude of these harmonics are of the order of 1.5% of the steady loads. When the centrifugal stresses are high as in the last stages of a machine, the dynamic stresses under resonant conditions can be sufficient to make cracks propagate.

Damping design is a crucial part of turbine blades. Without damping no blades can survive several criticals under transient conditions of startup and shutdown operations or near resonant conditions that may prevail in one or two blade rows of the machine near the steady operating speed. A little extra damping goes a long way in making the blades safer and that is what most turbine designers strive to provide in their systems. Blades essentially possess damping capacity from three different sources, viz., 1. Friction from slipping surfaces, 2. Material damping and 3. Aerodynamic damping. All these three damping mechanisms are complex and nonlinear in nature. Therefore, they cannot be individually modeled and summed up to give the net effect. Therefore, the equivalent viscous damping effect is popularly used to estimate the resonant stresses and is usually determined from spin tests with a single jet excitation.

Damping is found to be dependent on the root fixing effect caused by centrifugal forces, Coulomb damping at the interfacial surfaces, material damping and when the damping from these sources is very poor, aerodynamic damping from the flow path in the stage. Therefore, equivalent viscous damping is not constant for a blade, it is a function of speed of the machine, strain amplitude and the mode in which it is vibrating. Tests in this direction were conducted by Rao et. al.[13]. It is reported that multi jet excitation tests are now conducted in industry[14], to estimate the damping in a more accurate manner. The application of such nonlinear damping models to determine the modal response and resonant stresses is complicated, however, it gives accurate values when compared with tests, see[15].

The conventional procedure for life estimation is quite often based on high cycle fatigue theory. S-N and Mean Stress diagrams are coupled to define fatigue failure surface for the blade for specific conditions of operation. Such a procedure was adopted by Vyas and Rao[16] to determine the life of a turbine blade experiencing transient resonant conditions in terms of step-up and step-down operations. A program BLADE[17] is developed to estimate life of a free standing blade for Taipower company encompassing the above technologies. The input for such a program consists of stage geometry at different heights along the blade length, material properties, linear or nonlinear damping and operating conditions.

Though stress based life estimation procedures are useful at the preliminary design stages, life estimation based on fracture mechanics analysis is gaining importance since it considers fracture initiation, propagation and unstable fracture. Fracture mechanics analysis is usually based on two different approaches, 1. based on stress intensity factor and experimental data, see Barsom and Rolfe[18] and 2. based on local stress-strain approach, see Collins[19]. The stress intensity based approach primarily depends on extensive experimental data coupled with linear elastic fracture mechanics. This approach was used by Rao[3] in the fracture mechanics analysis of a last stage steam turbine blade. Though this procedure has been shown to be very practical, it suffers from the lack of experimental data for many materials that are commonly employed in many designs. Analytical procedures where possible have a distinct advantage and they use material properties which are generally available or easy to determine compared to a large amount of costly experimental data that is required for stress intensity factor approach. A combination approach is proposed by Dowling[20] and Socie et. al.[21] which involves strain life concepts to determine crack initiation life and linear elastic fracture mechanics principles to estimate crack propagation life. An application of such an approach was illustrated by Vyas, Sidharth and Rao[22] for beam type turbine blades. Rao et. al.[4] used the local stress-strain approach to investigate the cracking of Francis turbine runner blade cracks.

2. FRANCIS TURBINE RUNNER BLADE CRACK

2.1 Data:

Unit Rating	30 MW	
Net Head	Maximum	173.5 m
	Rated	146.5/165 m
	Minimum	139.0 m
Operating Speed	428.6 RPM	
Runaway Speed	875.0 RPM	
Inlet Runner Diameter	1.8 m	
Number of Guide Vanes (Nozzles)	16	
Number of Blades	11	
Runner Material	C<0.06, Si<1.0, Mn<1.0, Cr - 11.5 to 14.0, Ni - 3.0 to 5.0, Mo - 0.4 to 0.75, S<0.025, P<0.025	
Ultimate Tensile Strength σ_T	735 MPa	
Yield Strength σ_{ys}	590 MPa	
Young's Modulus E	193 GPa	
Percentage Reduction in Area (%RA)	40	
Cyclic Strength Coefficient K'	1730 MPa	
Cyclic Strain Hardening Exponent n'	0.14	
Fatigue Strength Coefficient σ_f'	$\sigma_T + 345 = 1080$ MPa	
Fatigue Ductility Coefficient ε_f'	$\ln \frac{1}{1-RA} = 0.51$	
Fatigue Strength Exponent b	-0.076	
Fatigue Ductility Exponent c	-0.62	

2.2. FEM Models

Each runner blade is defined using eleven board sections which are parallel to the crown or skirt. They are spaced equidistantly along the vertical turbine axis. These sections are drawn by feeding the coordinates of points on the section and joining them by 3-D spline. The blade is constructed by lofting through these sections. Crown and skirt are modeled by revolving the given cross-sections. The blade itself is copied at the eleven locations to obtain the runner CAD model. The solid model of the blade is shown in Fig. 2.1. The model is also checked by simulating the physical go and no-go test using balls of different diameters at different sections. These balls are modeled in I-DEAS and clearances verified at the respective locations.

A 3-D FEM model is developed by using SDRC I-DEAS Master series 2.1. The mesh is generated using tetrahedron elements. For frequency computations, linear tetrahedron elements are adopted and for stress computations, parabolic tetrahedron elements are used. The runner is treated fixed at the bolt locations by providing three translational restraints at these bolt locations. These boundary conditions are given in Fig. 2.2. For frequency run, the model has 10,137 nodes and 33,755 linear tetrahedron elements. For stress calculations, the model has 62,677 nodes with 33,642 parabolic tetrahedron elements. Fig. 2.3 gives the mesh with parabolic tetrahedron elements.

The fluid structure interaction problem in turbine blade vibration is quite complicated, see Gupta, Ramakrishnan and Rao[23]. The problem of modeling simple inviscid and incompressible fluid medium even for a single blade submerged under water is quite tedious and some form of simplification is adopted in the derivation of an added mass matrix to the general finite element problem. Obviously, this exercise becomes more complicated for several blades, the crown and the skirt if one considers the entire runner. Therefore a simplified procedure is adopted here in determining the natural frequencies; the entire mass of water volume contained within the runner is accounted for, while modeling the system. For simplicity, the density of the runner blade is altered by considering the total mass of the runner blade and water and dividing it by the runner volume alone.

2.3. External Force

The force acting on the blades has a frequency corresponding to the nozzle passing frequency equal to $16 \times \frac{428.6}{60} = 114.3$ Hz. For the nozzle passing frequency excitation, usually the first two harmonics are considered, therefore the excitation frequencies are 114.3 and 228.6 Hz. The pressure profiles in terms of meters of water column at the crown as well as skirt are given in [4] for both the pressure as well as suction sides. The pressure on the total surface is determined through data surface across the blade profile.

2.4 Natural Frequencies

The first six natural frequencies of the runner in water are obtained as

166.21 Hz	(1 ND Rigid Body Mode)
166.49 Hz	(1 ND Rigid Body Mode)
212.43 Hz	(I Bending Mode)
222.73 Hz	(II ND - I Bending Mode coupled with crown and skirt)
223.02 Hz	(II ND - I Bending Mode coupled with crown and skirt)
422.78 Hz	(Rigid Body Axial Mode)

The corresponding frequencies in air are 185.09, 185.99, 267.62, 268.77, 271.57 and 502.18 Hz respectively. We find that the second harmonic of the nozzle passing frequency is very close to the second nodal diameter modes with I bending of the blade and therefore this possibility of resonance is considered while estimating the crack initiation life.

2.5 Stresses

The stress field due to pressure profile considered as steady state is shown in Fig. 2.4. The peak stress is 117 MPa and the average von Mises stress is 17.12 MPa. The stresses due to centrifugal force at 428.6 RPM are given in Fig. 2.5. The peak stress is 37.6 MPa and the average von Mises stress is 7.58 MPa at a location on the blade-skirt junction which is farther from the turbine axis. The combined stresses due to steady load and centrifugal stress are shown in Fig. 2.6. The peak stress is 104 MPa and the average von Mises stress is 12.82 MPa. In all the cases, the peak stress occurred at a very narrow zone. The peak stress due to pressure profile alone or with the centrifugal force occurs in the junction of the crown and the blade on the inner surface.

The dynamic stresses in the present context arise from possible resonance of the plate bending mode with the second harmonic of the nozzle passing frequency. The second harmonic nozzle passing frequency excitation force is taken to be a maximum of 10% of the first harmonic, see [5]. Considering this magnitude of force as steady load, the peak stress is 12 MPa. Assuming a damping ratio of 0.02, see [5], the quality factor for fundamental bending is 25 and therefore the dynamic stress in a very narrow zone at the junction of the crown and the blade on the inner surface is $117 \times 0.1 \times 25 = 292.5$ MPa. The average von Mises stress in the runner blade is then $17.12 \times 0.1 \times 25 = 42.8$ MPa.

2.6. Local Stress Range

Making use of the relation between the total strain range $\Delta\varepsilon$, elastic strain range and plastic strain range, see [22]

$$\frac{\Delta\varepsilon}{2} = \frac{\Delta\sigma}{2E} + \left(\frac{\Delta\sigma}{2K'}\right)^{1/n'} \tag{2.1}$$

and Neuber's rule,[24]

$$\Delta\sigma\,\Delta\varepsilon = \frac{1}{E}(K_t \Delta S)^2 \tag{2.2}$$

the local stress range $\Delta\sigma$ at the point of stress raiser between the crown and the blade near the trailing edge can be obtained from

$$\Delta\sigma\left[\frac{\Delta\sigma}{E} + 2\left(\frac{\Delta\sigma}{2K'}\right)^{1/n'}\right] = \frac{1}{E}(K_t \Delta S)^2 \tag{2.3}$$

where ΔS is the nominal stress range and K_t is the stress concentration factor. The stress concentration factor is determined from the stress runs of the blade to be 5 and using the nominal stress estimated above, ΔS = 85.6 MPa, the above equation (2.3) yields

$$\Delta\sigma\left[\frac{\Delta\sigma}{193000} + 2\left(\frac{\Delta\sigma}{3460}\right)^{7.43}\right] = \frac{1}{193000}(5 \times 85.6)^2 \tag{2.4}$$

From the above, the local stress range is

$$\Delta\sigma = 426 \text{ MPa} \tag{2.5}$$

2.7. Local Strain Range

The local strain range from Neuber's rule is obtained as

$$\Delta\varepsilon = \frac{1}{\Delta\sigma E}(K_t \Delta S)^2$$
$$= \frac{1}{426 \times 193000}(5 \times 85.6)^2 = 0.0022 \tag{2.6}$$

2.8. Fracture Initiation Life

Making use of Basquin[25], Manson[26] and Coffin[27], the strain life equation is given by

$$\frac{\Delta\varepsilon}{2} = \frac{\sigma_f}{E}(2N_i)^b + \varepsilon_f'(2N_i)^c$$

(2.7)

Substituting the required material properties and the local strain range from equation (2.6), the number of cycles for fracture initiation, N_i, is given by

$$0.0011 = \frac{1085}{193000}(2N_i)^{-0.076} + \frac{0.73}{193000}(2N_i)^{-0.62}$$

(2.8)

i.e.,

$$N_i = 10^9 \text{ cycles}$$

(2.9)

Under pure resonant conditions, the life of the blade is

$$T_i = \frac{10^9}{228 \times 24 \times 3600}$$
$$= 50.76 \text{ Days}$$

(2.10)

It can be observed that the II ND runner frequency 222-223 Hz is very close to the second harmonic of the NPF 288 Hz. If the machine is run at constant operating speed 428.6 RPM, the dynamic stress induced in the runner will be slightly lower than that estimated under pure resonant conditions. However, it is known that the grid conditions in India are poor and there is quite often frequency excursions taking place beyond the specified limits. Such of these operating conditions accumulate resonances that are responsible for large dynamic stresses and when the accumulated period of such operations exceeds 51 days, fracture initiation takes place.

3. STEAM TURBINE LP BLADE CRACK PROPAGATION

The Narora machine is a 236 MWe nuclear turbine with one single flow HP and one double flow LP cylinder. There are five stages in the HP cylinder and five stages in each flow path of the LP cylinder. A schematic lay out of the machine is given in Fig. 3.1. Bearings #4 and #5 are mounted in the same housing. The machine was put on operation on 22nd March after a routine maintenance. The machine has put in 16,264 hours of operation and it experienced a total of 191 outages in its operation beginning from 29th July 1989.

3.1 The physical evidence (significant points) of the accident is listed below.

1. In all, sixteen LP V stage flow path 2 blades are found broken. Blades marked as #52 and # 51 failed at the blade root V-groove comes into contact with rotor disc top. Other nine blades #50 to #42 have broken at the tang portion.
2. All the lacing rods in this stage V are found missing.
3. Water catchment ring of stage 5 had all its bolts sheared and the rings are found to be severely damaged and displaced from their positions.
4. The nozzles of the fifth stage diaphragm had hit marks.
5. A puncture was observed in the outer casing apart from the hit marks.
6. Bearing #4 body was found broken into eight pieces. The babbit metal lining of the broken pieces was found to be more or less in tact showing least surface damage.

7. Both bearings #5 and #6 separated at their top and bottom halves and the white metal was more or less in tact.
8. Top half of generator inboard and outboard hydrogen seals were lying outside.
9. In the LP-Generator coupling, a few bolts are broken and came out. The coupling itself opened up by 8 to 10 mm.
10. LP shaft suffered a permanent bend of around 3 mm.
11. All bus bars are found melted and several bolts at the phase or neutral grounding bus are found loose from the debris.

3.2 The relevant records available prior to and during the accident time are as follows.

1. Turbine tripped at 03:31:40:005 hr and generator tripped after 105 ms at 03:31:40:110 hr.
2. Close to the time of tripping, feeder current in line 4 1R variation is found to be 300 amps.
3. Rotor coast down speed record, replotted for convenience and clarity given in Fig. 3.2 shows a hover at two speeds a minor one around 2700 and a major one around 1100 rpm.
4. Vibration records of all bearings except #4 are available. Bearing #5 in the same housing with #4, vibration levels are found to be on the high side, the record (replotted for convenience) since 30th March evening is shown in Fig. 3.3. All the other bearing vibration levels are under 30 microns.
5. Vibration levels recorded at some specific times from 22nd March are available. Bearing #5 recorded every evening since 25th March vibration levels of 100 microns in the axial direction. On 29th March these high levels upto 125 microns were observed for nearly five hours till midnight. The horizontal levels have also gone up 30 to 40 micron levels to 70 microns in this period.
6. As against a normal consumption of one to two cylinders of hydrogen, the set consumed 8 to 10 cylinders of hydrogen in the period 22nd March to 30th March 1997.
7. An earthquake laboratory 800 m away from the accident site recorded seismic activity during the turbine stopping period.

3.3. Blade Failure Scenario

Blade #52 had a clear fracture surface. Therefore, one suspects the first possible scenario of the machine accident to be the blade failure which causes heavy unbalance and the runaway situation causing the bearings and seals to fail and the resulting flames from the escaping hydrogen etc. An unbalance response calculation using linear bearing stiffness and damping coefficients is next made to determine the effect of loss of one blade in LP V stage flow path 2. The unbalance due to the loss of one blade is determined to be 220 Nm. The unbalance response values obtained are multiplied by 1.5, in the case of sudden loss of a blade. The maximum response occurred at the bearings #3, #1 & #4 in that order with amplitude values equal to 1700 microns.

Since the amplitude of the whirl is very large, it is obvious that the hydrodynamic bearing forces will be nonlinear and linear theories are no more valid. However, there are no established rotor dynamics codes with a large number of elements to take into account the nonlinear bearing forces. The non linearity in the bearing stiffness and damping forces will limit the amplitudes of

whirl to much lower orbital amplitudes than the linear theories. Even then, it can be expected that the amplitudes of whirl will be of the order of 1000 microns. However, the bearing clearances are of the order of 500 microns and therefore oil film will have to be squeezed out of the bearings #3, #1 & #4 and abnormal reactions will act at these supports.

As for the reaction forces, the results show that bearings #3 and #1 experience vertical dynamic loads which are 10 times that under static condition, whereas bearing #4 experiences an amplification of only 6. Bearing #5 is relatively unaffected. Since bearings #4 and #5 are in one casing, if a bearing fails, it should be bearing #3 followed by #1. There is neither any scoring of the babbit, nor bearings #3 and #1 failed in a catastrophic manner, therefore it is obvious that the blade is not lost at 3000 rpm normal running conditions when bearings #4 and #5 are still in tact.

Clearly the blade #52 failed in high cycle fatigue because of the presence of well defined crack propagation and unstable failure. SEM fractographs obtained by BHEL[28] confirms this failure mode. If the blade has not failed prior to the accident as an initiating event, then when did it fail and how did it fail? An answer to this question will further strengthen the premise that the blade failure is not the starting event of the accident.

3.4. Bearing Loss Scenario

The rotors when the machine is new have been balanced on the bearing pedestals to an accuracy of 2.5 to 5 microns. This corresponds to a quality less than G1 grade. Since the quality deteriorates with time, the rotors are assumed to have a quality equal to G2.5. Therefore, an eccentricity $e = Q/\omega = 2.5/314 = 0.00796$ mm is assumed. The steady unbalance response for 0.01 mm eccentricity is determined. The amplitude-eccentricity ratio in various unbalance configurations, is found to be less than 3 at all the bearing locations. The first four critical speeds under normal conditions are found to be 21.79 (Generator I mode), 31.35 (LP rotor I mode), 47.7 (HP rotor I mode) and 58.79 Hz (Generator II mode). The third mode of vibration of the system 47.7 Hz which belongs to predominant bending in HP rotor is the closest one to machine rpm, 50 Hz and the predominant bending of LP rotor is far away from the operating speed. The performance of bearings under normal conditions of operation is upto good design expectations.

The bearing #4 is lost in a catastrophic manner breaking itself into eight parts. Bearing #5 which is also housed in the same housing, broke into two halves at the parting planes. Examining the available vibration level records of bearing #5, it is clear that it is experiencing abnormal amplitudes practically every evening since the machine was put into service after the maintenance, see 3.2.5. During the evening of 30th March, the condition worsened and the vibration levels of bearing #5 indicate that it is practically bumping all the time, indicating that it is loose. In fact, it is the bearing #5 levels are those which shot up to levels beyond the range of the indicators at the beginning of the final failure of the machine.

Why would the bearings #4 and #5 fail first? According to Sohre[29] *"looseness" required to produce even the most violent vibrations may be microscopic, sometimes only a fraction of* 1/1000 *inch.* The two bearings under question are obviously loose and are bumping when the grid situations are unfavorable in the evening hours. The grid conditions in India are very poor, e.g., in the month of October 1992, the machine operated for over 70 hr. at frequency > 51 Hz and for over 50 hr. at frequency <49.5 Hz. If the bearings are loose, these frequency excursions create troublesome conditions for the machine. Moreover, the bus bars are found to have loose bolts and hydrogen has been excessively leaking into the duct area, see 3.1.11 and

3.2.6. Further, there has been an electrical unbalance right at the time the accident, see 3.2.2. The electrical unbalance with loose bolts and inflammable hydrogen and perhaps some transformer oil in the bus duct area could create a short circuiting type of conditions which jolt the machine severely. Such a condition can unseat the bearings and provide such a sudden load to break the loose bearing housings, e.g., the bearing #4 broke into eight pieces. Therefore, as the bearing #5 vibration level record indicates, bearings #4 and #5 have given way at the moment of the electrical unbalance. With this scenario, bearing loss calculations are performed as given below.

Hydrodynamic film forces, see[30], are first determined assuming stable whirl amplitudes equal to 50 microns. Because of the sudden loss of the bearings, twice the steady-state loads are applied at the respective bearing locations #4 and #5 for making equivalent static calculations using COSMOS finite element package. The results obtained at the bearing locations #4, #5, coupling and generator seal near the LP rotor end are given below.

Bearing-Loss Response - mm

Location	Horizontal Amplitude	Vertical Amplitude
Bearing #4	-9	3.3
Bearing #5	-11.13	2.1
Coupling	-9	2.9
Generator-Seal #5	-3.43	0.43

The response in the above table shows that plastic deformation should take place in the rotor system in the region of bearings #4 and #5. The present calculations are based on elastic theory. It was not possible at this stage to make combined elasto-plastic calculations. Due to the plastic deformation, a permanent set will occur. After the incident, the coupling is known to be opened by about 10 mm, see 3.1.9, which corroborates with the values obtained above. It was also observed that LP rotor suffered a permanent set by about 3 mm at bearing #4, see 3.1.10. The above elastic deformations at bearing #4 can yield such a permanent set. From the table above, it can also be seen that the generator seal near bearing #5 is subjected to heavy rubbing, which will result in an instantaneous escape of hydrogen.

To obtain the response in time domain, the bearing loads for 50 micron whirl are applied at the respective bearing locations #4 and #5 for a period of 7 milli seconds (one-third of a cycle). The instantaneous amplitudes of whirl are very large and in plastic region. The analysis is however based on elastic theory. The actual amplitudes of whirl can be much less than the values obtained from elastic theory. It is concluded that LP stage V in flow path 2, will be the first one to hit the water catchment ring. When the blades in LP V stage flow path 2 hit the water catchment ring, they will act as an additional support to the rotor. Assuming such a support, besides the bearings #1, #2, #3 and #6, the radial load transmitted to the water catchment ring is found to be 160 kN. The tangential force at the tip of the blade with a friction factor of 0.15 is therefore 24 kN. This force is used for calculation of stresses at the blade root.

The critical speeds after the loss of bearings #4 and #5 are next determined and in the coasting-down speed range they are 45.01, 18.26 and 4.21 Hz. The mode shape at 45.01 Hz (2700 rpm) shows that the LP stage V in flow path 2 is at a nodal point. If the blades are in tact

the unbalance is not severe, and the rotor coasts down smoothly without any blade rub with the casing. However, the resonance that takes place at 1095 rpm (18.26 Hz) causes very large amplitudes of whirl as LP stage V flow path 2 is at anti nodal point in this mode and the blades on this stage are subjected severe resonance. If the blades are lost at this stage, the unbalance becomes abnormally high. The rotor gets locked up at this critical speed for some time, which explains the hover observed at this speed range as shown in Fig. 3.4 and that it confirms that the two bearings #4 and #5 are not existent when the coast down speed is recorded.

3.5. When did Blade #52 Fail?

The blades in question are 12-14% Cr martensitic stainless steel. The last stage blades, 98 cm long, are provided with lacing rods, each rod passing through holes of two successive blades. Blades #52 and #51 in the LP V stage flow path 2 failed due to fatigue. Blade #53 has not failed but was subjected to cracks of small region. The remaining blades have failed in the airfoil section due to consequential effects. The fracture surface at first landing of the root of blade #52 is sketched in Fig. 3.4. The fractured surface could be divided into three distinct zones:

- Zone I - Primary fatigue fracture, where the crack propagated in a continuous manner with intermittent beach marks, after initiation at the sharp corner on the trailing edge. The striation spacing here is 0.1 to 0.3 microns.
- Zone II - Secondary fatigue fracture, where there were multiple fracture initiations on the trailing as well as leading edges of the blade. The striation spacing is 8 to 12 microns.
- Zone III - Final overload fracture.

The blade with the root is modeled by 43991 Parabolic Tetrahedron Solid elements with 74890 nodes[31]. The first bending mode at 3000 RPM is found to be 102.01 Hz very close to 2 per rev excitation 100 Hz. Steady stresses in the radial direction (for Mode I crack configuration) at the root are determined from the FEM analysis due to centrifugal load and steady steam bending. The steam bending stresses are found to be negligible in comparison to the centrifugal loads. The root is predominantly subjected to an average stress at the notch section of the first land equal to 318 MPa. (In the vicinity of the root fixing elements, very high stress values around 4000 MPa are seen in a depth of about a quarter of the edge element due to the existence of plastic conditions.)

The relation between the stress intensity factor ΔK and the stress range $\Delta\sigma$ is given by Barsom and Rolfe[29]

$$\Delta K = 1.12 \times 0.7 \times \Delta\sigma \sqrt{\pi a_T} \tag{3.1}$$

Crack Propagation:

A crack once initiated can propagate at a certain rate. For propagation to take place, a minimum threshold value of stress range is required. If the blade is subjected to stresses lower than this value then, even if a crack is initiated, it cannot propagate. Referring to Barsom and Rolfe[29], the threshold stress intensity factor for crack propagation is given by

$$\Delta K_{th} = 6.4(1 - 0.85R) \text{ ksi}\sqrt{\text{in}} \tag{3.2}$$

Taking $R = 68/386 = 0.176$,

$$\Delta K_{th} = 5.5 \text{ ksi}\sqrt{\text{in}} = 6 \text{ MPa}\sqrt{\text{m}} \tag{3.3}$$

From equation (3.1), $5.5 = 0.784\Delta\sigma\sqrt{0.281\pi}$ i.e., $\Delta\sigma = 7.46$ ksi = 51.5 MPa. Therefore, the crack can propagate only when the amplitude of stress is more than 25.75 MPa. Below this value of stress, even after crack initiation, the crack cannot propagate.

It is assumed that the blade is experiencing a pulsating force of 1% steady load[12] under transient excitations and that the damping is 0.5%, (i.e., quality factor = 100), the stress amplitude is determined to be 36.5 MPa, which is more than the threshold value above. Therefore, whenever transient excitation conditions (changes in frequency and load) exist, blade resonance takes place and the resulting stress amplitude is sufficient to propagate a crack that has been initiated. The fatigue-crack-propagation-rate data, Paris law, for martensitic steels from [29], is

$$\frac{da}{dN} = 0.66 \times 10^{-8}(\Delta K_I)^{2.25} \text{ in/cycle} \tag{3.4}$$

With $\Delta K_I = 1.12\sqrt{\pi}\,\Delta\sigma\sqrt{a_{avg}} = 1.98\Delta\sigma\sqrt{a_{avg}}$. Assuming $\Delta a = 0.05$ in, fatigue crack propagation rate equation is

$$\Delta N = \frac{0.05}{0.66\times10^{-8}\left(1.98\Delta\sigma\sqrt{a_{avg}}\right)^{2.25}} \tag{3.5}$$

Crack propagation in zone I is calculated for the stress range 10.59 ksi (73 MPa) which will take place whenever there are transient conditions of operations. The results are given in Fig. 3.5. The calculated striation spacing in Fig. 3.5 ranges from 0.05 to 0.25 microns. The striation spacing in this zone I from fractographic analysis is found to be 0.1 to 0.3 microns[32] which is in agreement with the above values. Therefore, it can be concluded that blade #52 with a crack initiated propagated over a length 1.575" in $\Sigma\Delta N = 282518$ cycles corresponding to 47 minutes of operation, whenever the stress amplitude is more than the threshold value, say, 36.5 MPa.

Fig. 3.4 shows that blade #52 suffered multiple fractures from the previous crack that existed at 40 mm length. For a fresh crack to initiate in 2000 cycles at a notch length of 1.57 in (corresponding to the first multiple crack mark), the stress intensity factor for a notch at the end of crack tip with 0.01 in radius, from Barsom and Rolfe[29], is

$$\Delta K_I = 400\sqrt{0.01} = 40 \text{ ksi}\sqrt{\text{in}} \tag{3.6}$$

The corresponding stress range from equation (3.1) is given by $40.0 = 0.784\Delta\sigma\sqrt{1.851\pi}$, i.e., $\Delta\sigma = 21.2$ ksi = 146 MPa. Hence, a stress amplitude of 73 MPa is sufficient to start a single fresh crack. The value of stress estimated under rub loads, however, is 296 MPa, which is far in excess of 73 MPa required to produce a single fresh crack. Hence, multiple cracks can initiate on blade #52 as actually observed. Therefore, it may be stated that the rubbing loads can cause fresh multiple cracks at the end of the previously existing crack on blade #52, however, on the rest of the blades, without any defect or blemish, the stress is not sufficient to start fresh cracks at the trailing edge This explains why blades other than #52 did not fail in fatigue fracture.

The response due to rub can be taken as double the stress values from static stress calculations. However, during the rub the blade may be free roughly half the time during these excursions. Therefore, on average a continuous dynamic response for stress range 296 MPa (43 ksi) is taken for the crack propagation calculation from 40 mm to 70 mm. Crack propagation in zone II for this load is also given in Fig. 3.5.

The striation spacing obtained in Fig. 3.5 is close to the actual values 8 to 12 microns found in zone II. The time taken for the crack to propagate from 40 mm to 70 mm under these conditions works out to 38 seconds with a blade natural frequency of 102 Hz. It is also noted that

there is a critical speed for the rotor 1095 rpm without the bearings #4 and #5. Therefore, the rubbing at this speed can be expected to be more severe than at other speeds during the excursions in the period of the accident when the rotor was decelerating from 3000 rpm to 0 rpm. Thus the observed failure of blade #52 can be attributed to the excessive loads experienced from the rubbing at 3000 rpm and in the subsequent periods in a time period less than 30 seconds as observed in the coast-down speed chart in Fig. 3.2.

Finally, the crack length to produce unstable conditions can be correlated with maximum stress and the fracture toughness for martensitic steels from the following relation, see[29]

$$a_f = \frac{1}{\pi}\left[\frac{K_c}{\sigma_{\max} F}\right]^2 \tag{3.7}$$

The fracture toughness of the material is $K_c = 210$ MPa$\sqrt{\text{m}}$ and the factor F is estimated as 1.3/1.125=1.16. Taking $a_f = 70$ mm, the maximum stress required for the observed fracture is given by $\sigma_{\max} = 386$ MPa. The average value of mean stress due to centrifugal forces and steam bending load at the cross-section of the fracture is 318 MPa. The amplitude of alternating component of stress needed therefore is 386-318 = 68 MPa, i.e., the alternating stress range is 136 MPa. The blade in practice however was subjected to loads of different magnitudes in its life time, transient resonance during rotor excursions and load fluctuations over a long period of time causing crack propagation in zone I and multiple loads over a short period of time in zone II. The above calculation can therefore be taken to represent an average situation.

The stress intensity factor at the final crack length observed can also be used to substantiate the blade fracture. The bending stress of the blade due to rubbing, when the blade has lost almost 50% area, is twice of 296 MPa, i.e., 592 MPa. In addition, centrifugal stress at 1100 rpm with around 50% area is determined as 85 MPa. The total stress is thus 677 MPa (98 ksi). The stress intensity factor is then [29] $K = 1.12 \times 0.7 \times 98.0 \times \sqrt{2\pi} = 193$ ksi$\sqrt{\text{in}} = 230$ MPa$\sqrt{\text{m}}$ .This value being more than the fracture toughness of the material, the failure of blade #52 takes place as observed.

4. REFERENCES

[1]Fleeting, R. and Coats, R., Blade Failure in the HP Turbines of RMS Queen Elizabeth 2 and Their Rectification, *Trans Institution of Marine Engineers*, 1970, p. 49

[2]Frank, W., *Schaden Spiegel*, vol. 25, #1, 1982, p. 20

[3]Rao, J. S., Fracture Mechanics Analysis of A Steam Turbine Blade Failure, *Proc.* 1995 *Design Engng Technical Conferences, ASME*, DE-Vol. 84-2, p. 1173, September 17-21,1995, Boston

[4]Rao, J. S. et. al. Application of Local Stress-Strain Approach to Predict Fracture Initiation of A Francis Turbine Runner Blade, ISROMAC-7 conference, Hawaii, February 22-26, 1998

[5]Rao, J. S., *Turbine Blade Vibration*, John Wiley and Sons, 1992

[6]Rao, J. S., Subrahmanyam, K. B. and Kulkarni, S. V., Coupled Bending Torsion Vibrations of Rotating Blades of Asymmetric Airfoil Cross-section Allowing for Shear Deflection and Rotary Inertia by Reissner Method, *J Sound Vib*, v.75, 1981, p.17

[7]Hohlreider, M. and Irretier, H., TUBSIM - A Computer Program Package for Forced Vibrations and Life Estimation of Turbine Blades for Stationary and Transient Operations, *Proc. I. Mech. E. Conf. Vibrations in Rotating Machinery,* 1992, p. 21

[8]Bahree, R. Sharan, A. M. and Rao, J. S., The Design of Rotor Blades due to the Combined Effects of Vibratory and Thermal Loads, *J Engng. Power and Gas Turbines,* v. 111, 1989, p. 610

[9]Rao, J. S., Ramakrishnan, C. V., Gupta, K. and Rao, K. K., Vibration Analysis of Rotating Cambered Helicoidal Turbomachine Blades, *ASME 97-GT-299*, Orlando
[10]*SDRC I-DEAS Master Series 4*, 2000 Eastman Drive, Milford, Ohio
[11]Rao, J. S., *Turbomachine Unsteady Aerodynamics,* Wiley Eastern, 1994
[12]Levin, A., *Moving Blades and Disks of Steam Turbines*, The State Power Engineering Publishers, 1953, Moscow (In Russian)
[13]Rao, J. S., Gupta, K, and Vyas, N. S., Blade Damping Measurement in A Spin Rig with Nozzle Passing Excitation Simulated by Electromagnets, *Shock & Vib Bull*, 56, Pt 2, 1986, p.109
[14]Benedict, B., ASME Professional Development Program *Forced Vibration of Blades and Life Prediction,* 5/31/97-6/1/97, Orlando - Instructor J. S. Rao
[15]Rao, J. S. and Vyas, N. S., Determination of Blade Stresses under Constant Speed and Transient Conditions with Nonlinear Damping, *J of Engng for Gas Turbines and Power, Trans ASME*, vol. 118, No. 2, 1996, p. 424
[16]Vyas, N. S. and Rao, J. S., Fatigue Life Estimation Procedure for a Turbine Blade Under Transient Loads, *J of Engng for Power and Gas Turbines, Trans ASME*, v. 116, 1994, p. 198
[17]Rao, J. S., Vyas, N. S. and Liu-De Shin, *Life Estimation of Turbine Blades*, Tai power Co., Taipei, 1996
[18]Barsom, J. M. and Rolfe, S. T., *Fracture and Fatigue Control in Structures*, Prentice Hall, 1987
[19]Collins, J. A., *Failure of Materials in Mechanical Design*, John Wiley and Sons, 1981
[20]Dowling, N. E., Fatigue at Notches and the Local Strain and Fracture Mechanics Approaches, *Fracture Mechanics*, ASTM STP 677, ed. C. W. Smith, pp. 247-273, 1979
[21]Socie, D. F. Dowling, N. E. and Kurath, P., Fatigue Life Estimation of Notched Members, *Fracture Mechanics*, 15th Symposium, ed., R. J. Sanford, ASTM STP 833, pp. 284-299, 1984
[22]Vyas, N. S., Sidharth and Rao, J. S., Dynamic Stress Analysis and A Fracture Mechanics approach to Life Prediction of Turbine Blades, *Mechanism and Machine Theory*, v. 32, No. 4, 1997, p. 511
[23]Gupta, D. K., Ramakrishnan, C. V. and Rao, J. S., Fluid Structure Interaction Problems in Turbine Blade Vibration, *Recent advances in Fluid Structure Interaction, ASME Publication*, p. 89, 1984
[24]Neuber, H., Theory of Stress Concentration for Shear-Strained Prismatical Bodies with Arbitrary Nonlinear stress Strain Laws, *J. Appld. Mech., Trans ASME*, vol. E28, p. 544, 1964
[25]Basquin, O. H., The Experimental Law of Endurance Tests, *Proc. ASTM*, vol. 10, p. 625, 1910
[26]Manson, S. S., Behaviour of Materials under Conditions of Thermal Stress, *Heat Transfer Symposium, University of Michigan, Engng. Res. Inst.*, p. 9-75, 1953
[27]Coffin, L. F. Jr., A Study of the effects of Cyclic Thermal Stresses on a Ductile Material, *Trans ASME,* vol. 76, p. 931, 1954
[28]SEM Fractographic Test Results, *Personal Communication*, BHEL R&D, Hyderabad
[29]Sohre, J. S., Turbomachinery Problems and Their Correction, *Standardization and Condition Monitoring Workshop*, March 11-13, 1991, chapter 7
[30]Rao, J. S., *Rotor Dynamics*, 3rd Edition, New Age International, 1996
[31]Narora Blade Model Results, *Private Communication*, BHEL ARP Division, New Delhi
[32]Fractographic Analysis Results, *Personal Communication*, BARC, Bombay

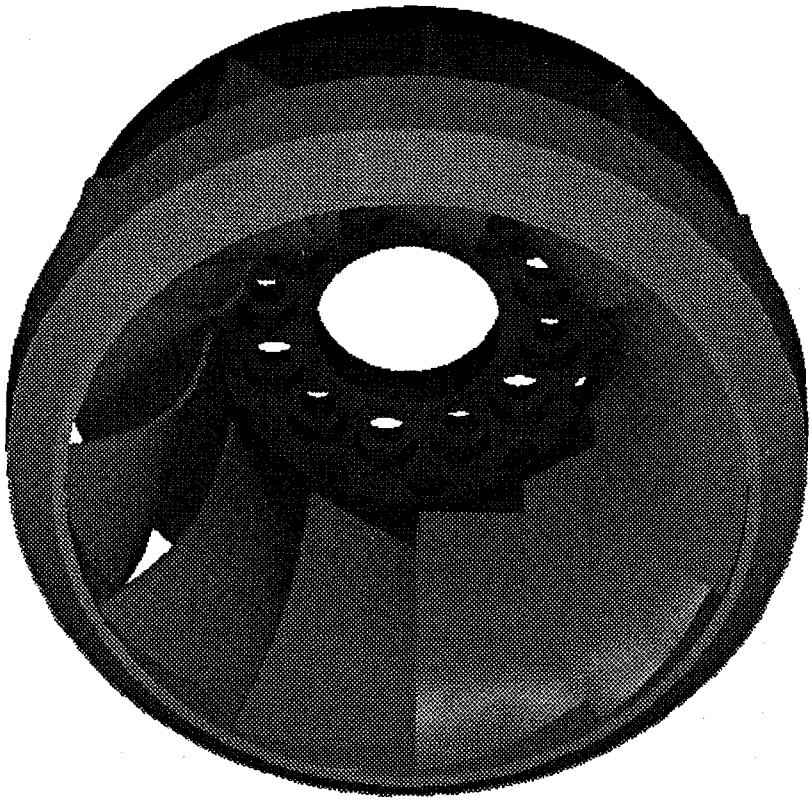

Fig. 2.1 CAD Solid Model of Turbine Runner

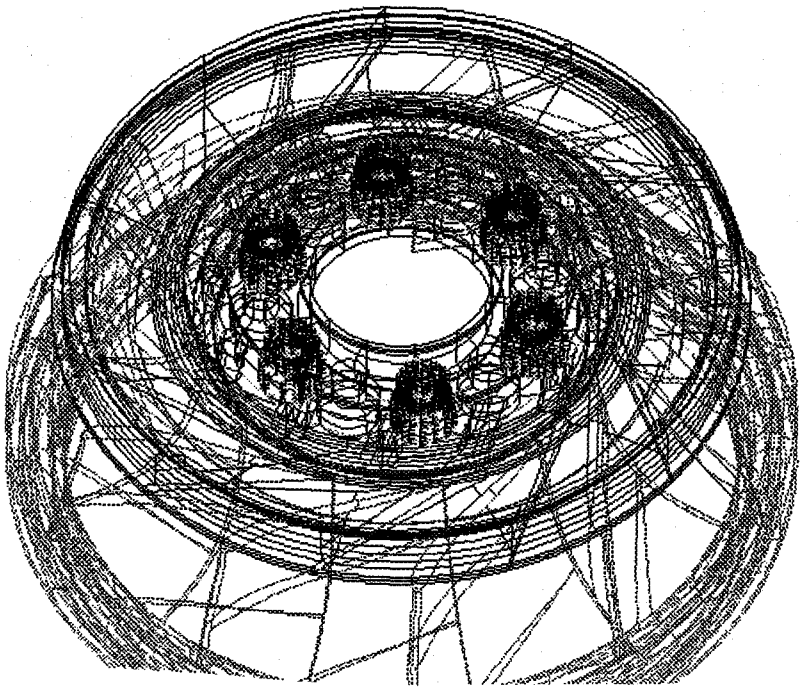

Fig. 2.2 Boundary Conditions

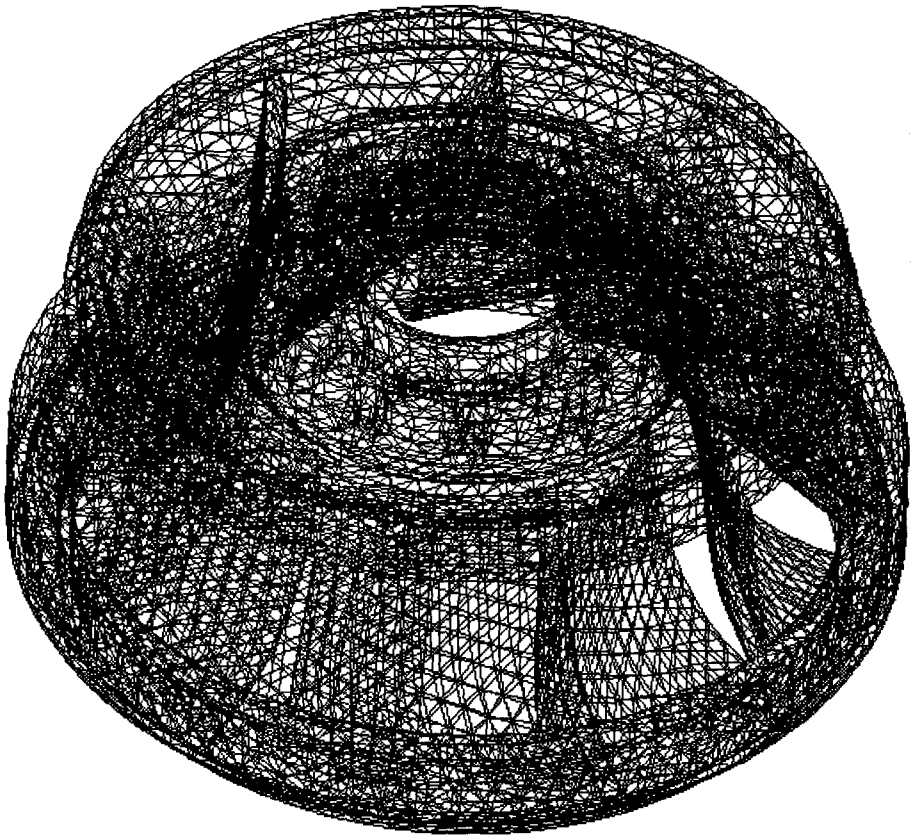

Fig. 2.3 Finite Element Mesh

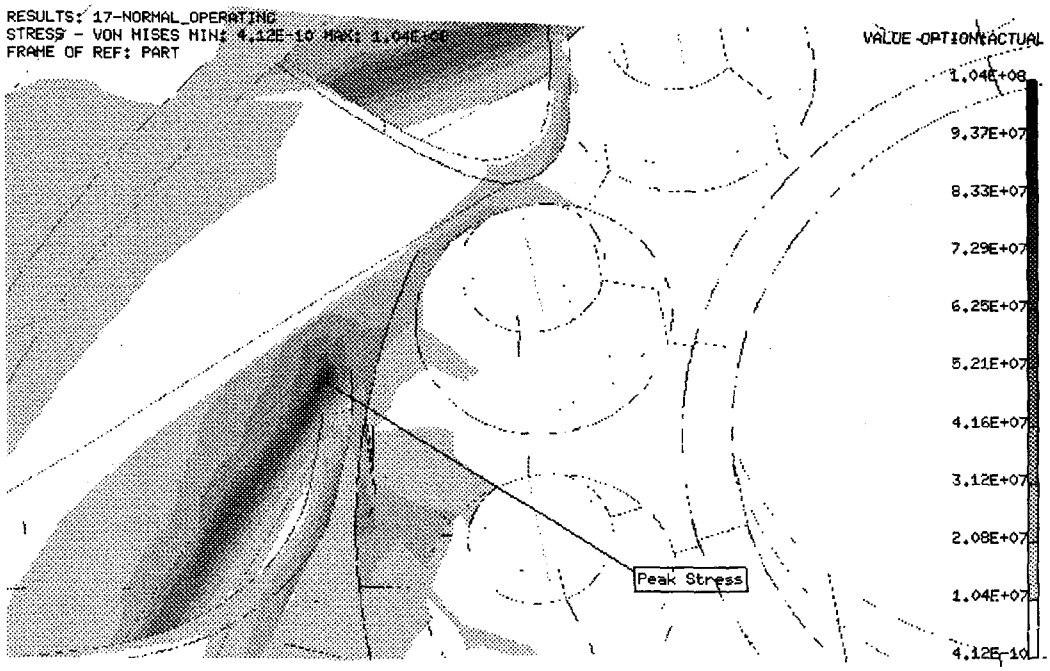

Fig. 2.4 Stress Due to Pressure

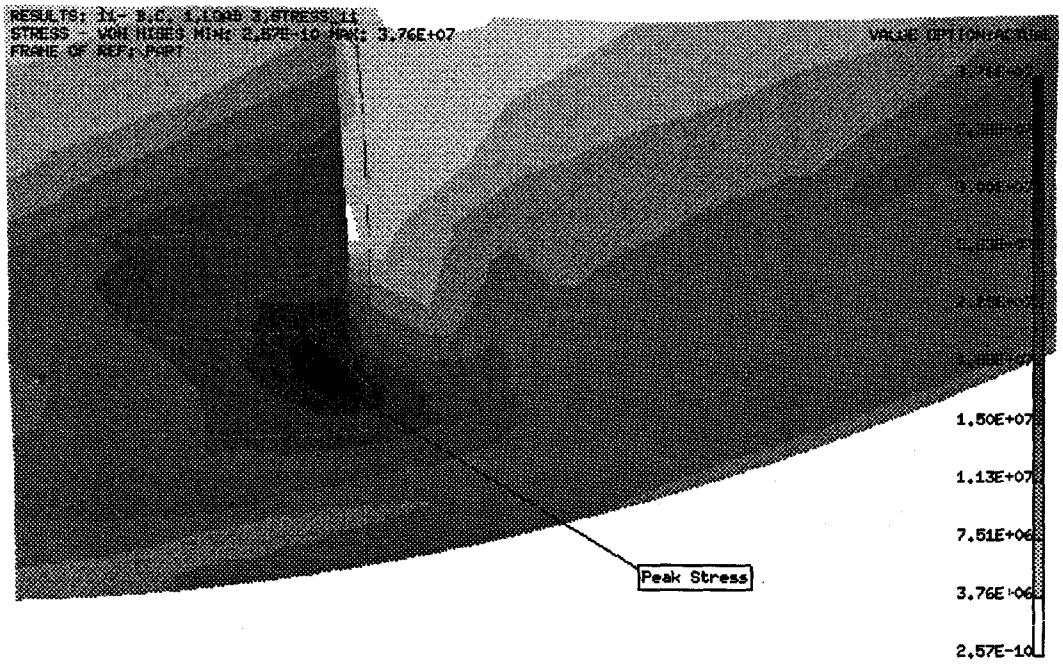

Fig. 2.5 Stress Due to Centrifugal Force

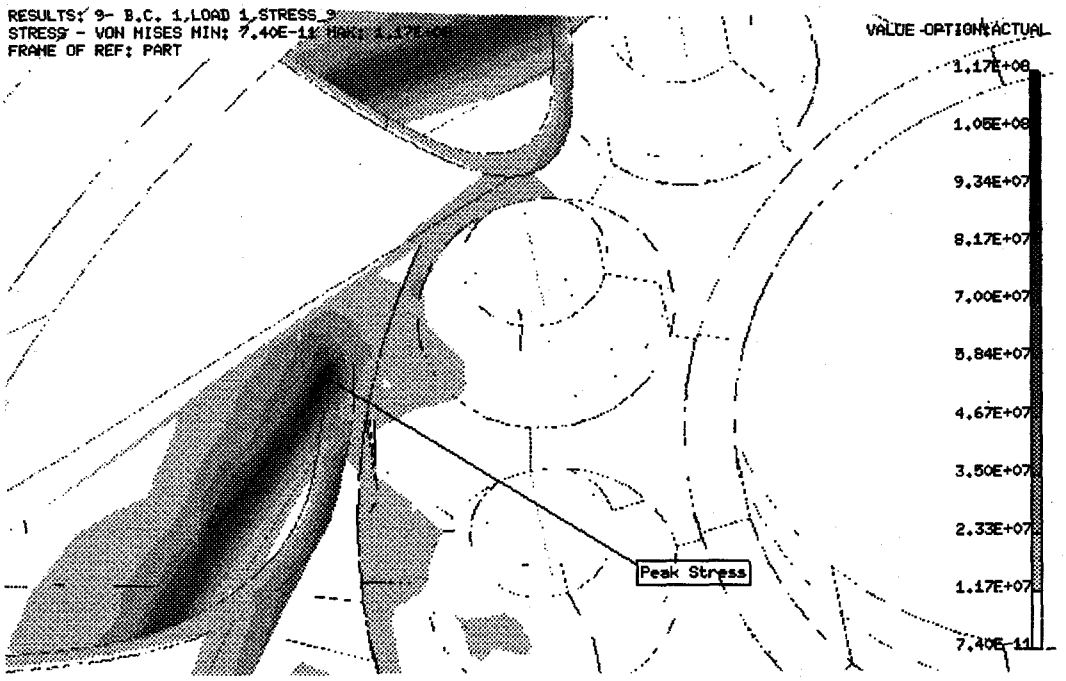

Fig. 2.6 Stress Due to Pressure and Centrifugal Force

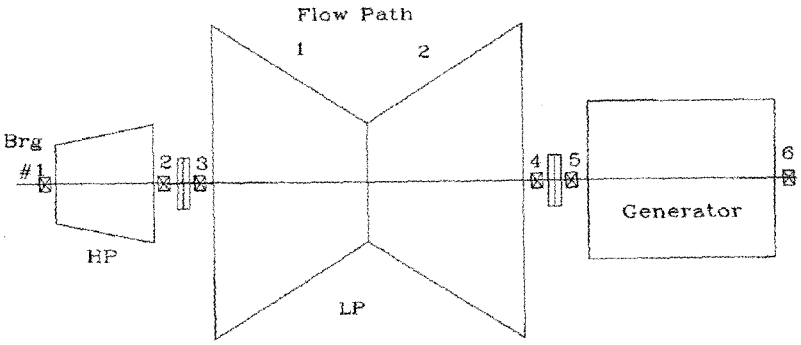

Fig. 3.1 Arrangement of 236 MW Turbo-Generator Set

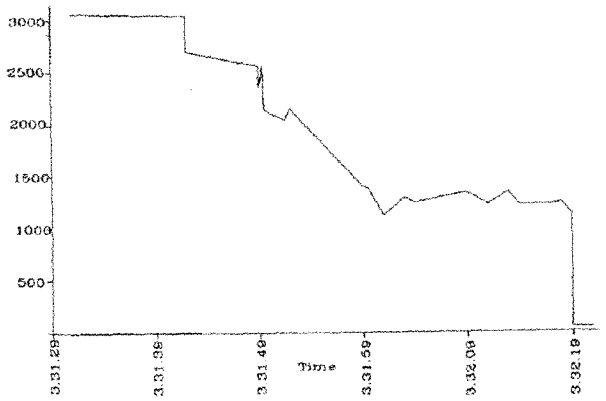

Fig. 3.2 Coasting Down Speed

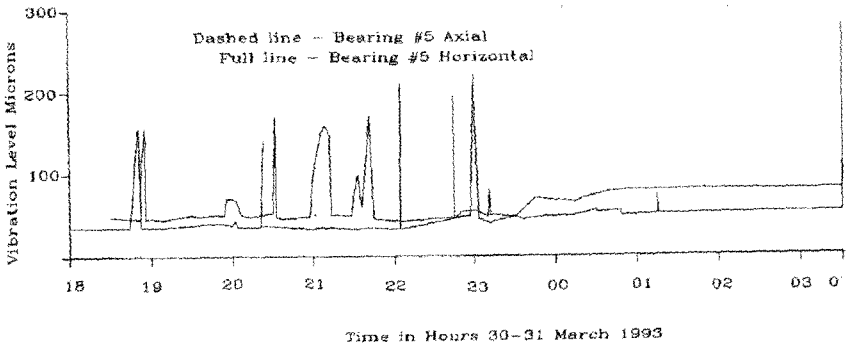

Fig. 3.3 Vibration Level Record of Bearing #5

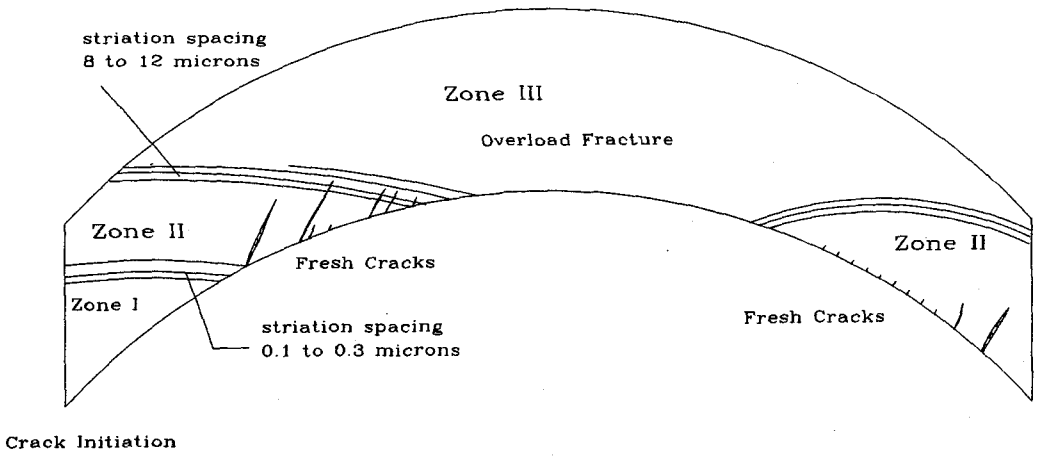

Fig. 3.4 Three Zones of Fracture in Blade #52

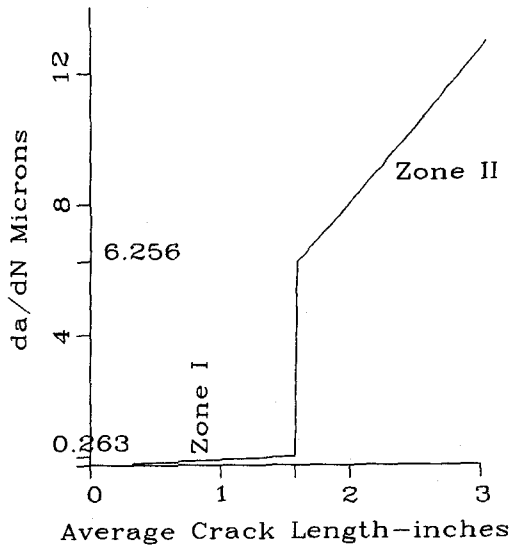

Fig. 3.5 Crack Growth in Zones I and II